

The Uptake Potential of Santa Barbara Amorphous Silica/Zeolite Composite for Environmental Microplastics in Wastewater

Martins O. Omorogie* and Brigitte Helmreich



Cite This: *ACS EST Water* 2024, 4, 5447–5460



Read Online

ACCESS |



Metrics & More



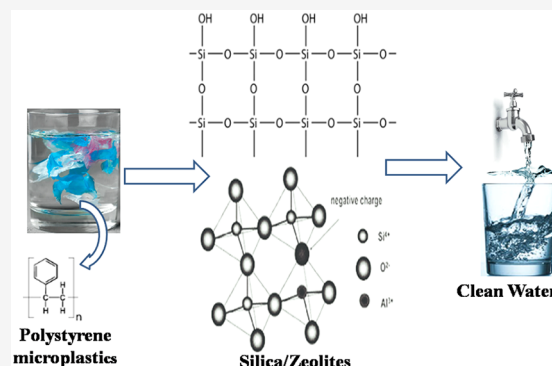
Article Recommendations



Supporting Information

ABSTRACT: Recently, the challenge of environmental microplastics (enMPs) in ecosystems has become a serious global concern. This is because the transport of enMPs has been known as a precarious culprit in depleting ecosystems, likely decreasing life expectancy, reducing the quality of human life, and threatening the future survival of fauna and flora. This menace is seriously threatening the continued existence and well-being of all biomes. Hence, this research attempts to provide a panacea to this global environmental issue through the application of Santa Barbara Amorphous silicas/zeolite composite (SSZC) for the removal of polystyrene microplastics (PMPs) from water and wastewater. This research showed that the adsorption capacity of SSZC for PMPs was $2.41 \text{ mg}\cdot\text{g}^{-1}$. This was achieved by chemisorption between SSZC and PMPs via electrostatic attraction and hydrophobic interactions, such as covalent bonding, noncovalent aromatic π -system, and electron donor–acceptor interactions. The surface morphology of SSZC showed that C–H, C–O, C=C, N–H, Al–O, Si–O–Si, and Si–OH were the functional moieties present on its surface and available for adsorption.

KEYWORDS: polystyrene, microplastics, water/wastewater treatment, SBA 15 silica, SBA 16 silica, zeolite



1. INTRODUCTION

The global industrial revolution over the past seven decades has led to the ubiquitous applications of plastics as a versatile and cost-effective material for food, packaging, textiles, construction, agro, and other industries. This extensive use of plastics has increased their production from 1.7 million tons in 1950 to 368 million tons in 2019. If appropriate plastic waste management is globally enforced, then production is expected to increase to 445 million tons by 2025. Hence, statistical projections have shown that this figure might increase by 29% by 2028. Mismanagement and improper disposal of plastic products in the environment trigger their release into the aquatic ecosystem as fragments after their exposure to ultraviolet radiation, mechanical abrasion, chemical degradation, and thermal degradation into minuscule plastic debris that float as microplastics (MPs) and nano-plastics into streams, rivers, seas, and oceans.^{1–8}

The presence of MPs in the environment has become a major global concern due to their emerging adverse effects on humans and animals, including weakened immune systems, DNA damage, high oxidative stress in humans, and toxicological hazards in aquatic organisms and other animals.^{2,3,9} Over the past decade, MPs have posed a serious threat to the future existence of humans, fauna, and flora. Thus, urgent attention is needed to address this threat and provide a

swift solution to this environmental challenge, preventing further damage to the ecosystem.

The aforementioned adverse effects of microplastics in the ecosystem have drawn the attention of researchers worldwide in recent years. Significant efforts have been made to combat this serious environmental challenge through various biological, chemical, and physical methods. For instance, researchers globally have conducted studies on the environmental presence, monitoring, impact and assessment of microplastics in water. A bibliometric search on Clarivate Analytics Web of Science using the title “Microplastics” revealed that 15,956 papers so far have been published and indexed in Web of Science Core Collection. However, another bibliometric search on Clarivate Analytics Web of Science using the title “Removal of microplastics in water by materials” revealed that over 100 papers have been published and indexed in the Web of Science Core Collection, with at least 30 of these being review and research papers on the qualitative analysis of plastics/plastic additives (retrieved from Clarivate Analytics

Received: June 18, 2024

Revised: October 31, 2024

Accepted: October 31, 2024

Published: November 12, 2024



Web of Science on 17 September 2024). Researchers have been able to deduce various qualitative profiles of microplastics in different regions of the world using various sampling techniques. It is interesting to note that the qualitative profiling of microplastics in water bodies around the world has only been successful in detecting their presence, leaving out their quantification in water. In this context, the effective quantification of microplastics in water remains a serious challenge for the research community. Driven by this, our research aims to explore the application of facile spectrophotometry for the quantification of microplastics in contaminated water and wastewater.

Literature has shown that researchers have employed some expensive and laborious materials that are nonbenign for the removal of MPs via membrane filtration, density concentration and magnetic extraction, advanced oxidative processes, microbial degradation, coagulation, and adsorption.^{10–23} However, these methods have some drawbacks, such as membrane fouling, the use of large quantities of coagulants, the release of secondary byproducts and chemical intermediates, low efficiency, high cost, nonsimplistic, and nonbenign and nonfacile processes, with the exception of adsorption.^{10–15,24,25} Irrespective of the fact that most materials are not cost-effective, unsustainable, and difficult to synthesize, they are not easily recycled after one or two experimental runs. This is because their active sites are easily blocked due to the availability of small-sized pores that lead to poor internal and external adsorption. Zeolites are aluminosilicate monolithic materials with a defined structure, relatively stable characteristics under humid conditions, permanent porosity, and highly ordered crystals. Due to their defined structure, they contain interconnecting cavities that can be used for the entrapment of target molecules of interest. They possess a good proportion of ecofriendly silicate/aluminate ($\text{SiO}_2/\text{Al}_2\text{O}_3$), which gives them a distinctive affinity for hydrophobic molecules (polar compounds) and low affinity for hydrophilic compounds (non polar compounds). These features are responsible for the improved external and internal adsorption performance of zeolites.^{26–30} Also, Santa Barbara Amorphous (SBA) silicas are monoliths with stable pore sizes, excellent stability, good dispersibility in water, favorable recovery characteristics, and relatively low cost compared to many other materials.³¹ Thus, the amalgamation of zeolites and SBA silicas will produce a composite with good and feasible adsorption capabilities, ecofriendliness, and recycle/recovery potential, promoting the sustainability of adsorbents. Based on the aforementioned, we synthesized a facile and eco-friendly composite material from zeolites, Pluronic *p*-123 (SBA 15), and Pluronic F-127 (SBA 16) silica (SSZC) for the removal of polystyrene microplastics (PMPs) from water and wastewater.

2. MATERIALS AND METHODOLOGY

All chemicals were obtained from commercial sources and used without further purification.

2.1. Synthesis of Santa Barbara Amorphous Silica/Zeolite Composite (SSZC). SSZC was synthesized according to the modified protocol of Omorogie et al.³² Typically, 5 g each of Pluronic *p*-123 and Pluronic F-127 were dissolved in 400 mL of deionized water (Millipore, electrical resistivity of 18.2 M Ω -cm at 23 °C) and stirred vigorously at room temperature for 30 min with a magnetic stirrer at 1200 rpm, leading to a transparent solution. To this transparent solution was added 50 mL of tetraethyl orthosilicate (TEOS) (Merck,

KGaA, Germany) gradually, followed by 25 mL of 0.1 M NaOH stepwise. The obtained white suspension was left under magnetic stirring conditions for 3 h. After 3 h, this white suspension was decanted and centrifuged at 3,000 rpm for 10 min (Multi-application Centrifuge, NUWND Model, Germany) to obtain the supernatant. Then, the white paste was dried in an oven (ThermoFisher Scientific GmbH, Germany) at 100 °C for 36 h to remove moisture. After that, the white paste was placed in porcelain crucibles and heated at 550 °C in a muffle furnace (Carbolite, CWF 1100 Model (Merck, KGaA, Germany) for 3 h with a ramp of 30 °C min⁻¹. The obtained white solid was cooled to room temperature and stored in a desiccator for experimental use.

2.2. Preparation of PMP Suspension for Adsorption and Desorption Studies. The analytical standard of 6 μm of monodispersed PMP suspension with a specific gravity of 1.05 g·cm⁻³ (Sigma-Aldrich Chemie GmbH, Germany) was sonicated in an ultrasonic bath (Bandelin Electronic GmbH and Co. KG, Germany) for 15 min, to enhance their dispersion in 1:1 deionized (Millipore, electrical resistivity of 18.2 M Ω -cm at 25 °C) water/ethanol mixture. After sonication, the standard PMP solution was diluted into various experimental concentrations. Adsorption studies were done in triplicate, with 100 mg each of SSZC added to 25 mL of 10 mg·L⁻¹ of PMPs adjusted to pH values of 2.0 to 12.0 (pH studies), with initial concentrations of 1.0 to 10 mg·L⁻¹ (equilibrium studies), agitation times of 1 to 180 min (kinetic studies), temperatures of 25 to 55 °C (thermodynamic studies), and adsorbent masses of 0.5 to 1.25 g (adsorbent dose). SSZC was used for the recycling study using 0.1 M nitric acid, acetone, deionized water, and ethanol for 3 h at 200 rpm for five cycles at 25 °C. Some samples of drinking water (DGW) and wastewater (WEW) from WW Treatment Plant in Garching (48° 15'N 11° 39'E), Germany, were collected and spiked with 1 mg·L⁻¹, 4 mg·L⁻¹, and 10 mg·L⁻¹ of PMPs, respectively. Fifty milligrams of SSZC was added to 25 mL of these spiked solutions and agitated for 3 h at 200 rpm. The WEW was characterized by chemical oxygen demand (COD), biochemical oxygen demand over 5 days (BOD₅), total dissolved solids (TDS), total suspended solids (TSS), electrical conductivity (EC), and turbidity.

Supernatants from all experimental samples were centrifuged (Multi-application Centrifuge, Germany) at 5,000 rpm for 12 min and analyzed for PMP concentrations by a UV/Visible Spectrophotometer (DR 6000 Model, Hach Lange GmbH, Düsseldorf, Germany). The quantities of PMPs adsorbed (q_e) by SSZC in mg·g⁻¹ were calculated by the mass balance equation, given as

$$q_e = \left\{ (C_i - C_e) \times \frac{v}{m} \right\} \quad (1)$$

where C_i , C_e , v , and m are expressed as the initial concentration of adsorbate ions (mg·L⁻¹), equilibrium concentration of adsorbate ions (mg·L⁻¹), volume of aqueous solutions (L), and mass of adsorbent (g), respectively.

Experimental data from equilibrium, kinetic, and thermodynamic studies were fit into two-parameter nonlinear equations,³² optimized by Data Analysis and Graphing Software, OriginPro 9.1, OriginLab Corporation, Northampton, Massachusetts, USA, and Quasi-Newton least-squares algorithm and the correlation coefficient (R^2) in a KyPlot Software 2.0 model (KyensLab Incorporated, Tokyo, Japan). These are given as

$$q_e = K_{Fr} C_e^{1/n} \quad (2)$$

Freundlich model (FM)³³

$$q_e = \frac{q_{m,La} K_{La} C_e}{1 + K_{La} C_e} \quad (3)$$

Langmuir model (LM)³⁴

$$q_t = q_e (1 - e^{-k_t t}) \quad (4)$$

Pseudo first order (PFOM)³⁵

$$q_t = \frac{k_2 q_e^2 t}{1 + k_2 q_e t} \quad (5)$$

Pseudo second order (PSOM)³⁶

$$\ln\left(\frac{k_2}{T}\right) = \ln\left(\frac{k^*}{h}\right) + \left(\frac{\Delta S^\circ}{R}\right) - \left(\frac{\Delta H^\circ}{RT}\right) \quad (6)$$

Eyring model³⁷

K_{Fr} , n , K_{La} , $q_{m,La}$, q_e , k_1 , k_2 , ΔS° , ΔH° , R , K^* , h , and T are Freundlich constant ($\text{mg}\cdot\text{g}^{-1}$)($\text{L}\cdot\text{mg}^{-1}$)^{1/n}, Freundlich empirical constant that depicts the adsorption affinity, Langmuir adsorption constant ($\text{L}\cdot\text{mg}^{-1}$), q_e for a complete monolayer ($\text{mg}\cdot\text{g}^{-1}$), amounts of adsorbate ions adsorbed at time t (min) by SSZC ($\text{mg}\cdot\text{g}^{-1}$), pseudo-first-order rate constant (min^{-1}), pseudo-second-order rate constant ($\text{g}\cdot\text{mg}^{-1}\cdot\text{min}^{-1}$), entropy change ($\text{J}\cdot\text{mol}^{-1}\cdot\text{K}^{-1}$), enthalpy change ($\text{J}\cdot\text{mol}^{-1}$), universal gas constant ($8.314 \text{ J}\cdot\text{mol}^{-1}\cdot\text{K}^{-1}$), Boltzmann constant ($1.381 \times 10^{-23} \text{ J}\cdot\text{K}^{-1}$), Planck constant ($6.626 \times 10^{-34} \text{ J}\cdot\text{s}$), and absolute temperature (K), respectively.

2.3. Characterization of Surface Textural Properties of SSZC. Attenuated total reflectance-infrared (ATR-IR) spectrophotometry was performed using a PerkinElmer Spectrum 100 ATR-IR spectrometer with a Specac Golden Gate ATR unit. The background was obtained using potassium bromide, and the scanning wavenumber range was from 400 to 4,000 cm^{-1} . Scanning electron microscopy–energy-dispersive X-ray spectroscopy (SEM-EDX) was performed using a SIGMA VP 300 (Carl Zeiss AG, Germany) microscope. Images and spectra were recorded with the In-Lens detector at an acceleration voltage of 1.00–2.00 kV with a working distance between 2.8 and 3.1 mm. The thermogravimetric analysis (TGA) and differential thermogravimetry (DTG) were studied by a NETZSCH STA 449F3 Jupiter. The Al_2O_3 crucible was used for these analyses with a heating rate of 10 $^\circ\text{C}\cdot\text{min}^{-1}$ from ambient temperature to 1,000 $^\circ\text{C}$. The X-ray diffraction (XRD) analysis was performed using a Bruker D8 Bragg–Brentano Geometry, with $\text{Cu K}\alpha$ radiation ($\lambda = 0.154 \text{ nm}$) at 40 kV and 40 mA. SSZC was ground in 2-propanol and dried in a vacuum compartment dryer at 40 $^\circ\text{C}$ before measurement. N_2 adsorption/desorption physisorption was performed using a Microtrack Belsorp Mini 2 physisorption meter. SSZC was degassed at 10 Pa and 200 $^\circ\text{C}$ for 3 h before the measurements were conducted. The Brunauer–Emmett–Teller (BET) and T-plot multipoint techniques were used to analyze the specific surface area and pore structure of SSZC.

The solid-state magic angle spinning-nuclear magnetic resonance (MAS NMR) was recorded by a Bruker Avance 300 model spectrometer (magnetic field strength 7.0455 T, resonance frequency of ^{27}Al : 78.12 MHz and ^{29}Si : 59.63 MHz). SSZC was packed in 4 mm zirconia rotors for the ^{27}Al

(spinning rate: 15 kHz) and in 7 mm zirconia rotors for ^{29}Si NMR measurements (spinning rate: 5 kHz), both spun at MAS. For the ^{27}Al measurements, 2000 scans were taken with a repetition time of 0.5 s, and the chemical shifts were set relative to aluminum hydroxide. The ^{29}Si spectra were recorded with a repetition time of 45 s, and over 2000 scans were taken. The chemical shifts were recorded relative to tetramethylsilane for ^{27}Al and ^{29}Si MAS NMR experiments with a single pulse technique. A zetasizer from Dispersion Technology Model DT 1200 was used for the zeta potential measurement of SSZC. The spectra from X-ray Photoelectron Spectroscopy (XPS) were obtained in the hybrid lens mode at a pass energy of 10 eV and a takeoff angle of 0 $^\circ$ with a Kratos Axis Supra setup equipped with a monochromatic $\text{Al K}\alpha$ X-ray source ($h\nu = 1486.7 \text{ eV}$) operated with an emission current of 15 mA and an applied power of 225 W. The beam area was set to $\approx 2 \times 1 \text{ mm}^2$ using the slot collimation mode to characterize SSZC.

3. RESULTS AND DISCUSSION

3.1. Characterization of SSZC. Detailed discussions on zeta potential (ZP), thermogravimetry (TG) and differential thermogravimetry (DTG), attenuated total reflectance-infrared (ATR-IR) spectrophotometry and ^{27}Al and ^{29}Si solid-state magic angle spinning-nuclear magnetic resonance (MAS-NMR) for SSZC and PMPs-SSZC are available in Sections S1–S4 and Figures S1–S4.

3.1.1. X-Ray Diffraction (XRD) of SSZC. XRD gives scientific information about the physicochemical properties and crystal structure of materials. For XRD analysis, materials comprise different phases that produce unique diffraction patterns that typify their specific chemistry and atomic arrangement(s).³⁸ Figure 1 shows the XRD pattern of SSZC, which reveals

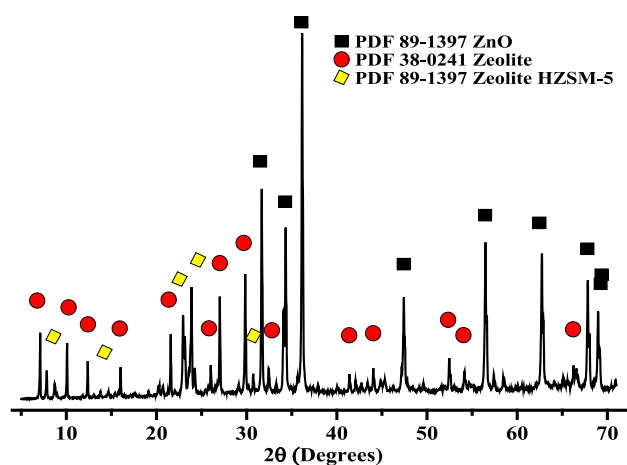


Figure 1. The XRD pattern of SSZC.

various peak indices at $2\theta = 7.1^\circ$, 10.3° , 23° , 24° , 27° , and 30° , corresponding to the (101), (200), (332), (303), and (133) planes of the zeolite, respectively. The peak indices at 23° and 24° indicate that the structure of the zeolite is orthorhombic in nature.³⁹ Moreover, the peak indices at $2\theta = 32^\circ$, 34° , 47.4° , 56.5° , 68° , and 69° represent (111), (200), (220), (311), (400), and (311) planes of silica, respectively. These peak indices for silica are typical for SBA 15 and 16 silica structures, which possess characteristic tiny aggregated particles. This

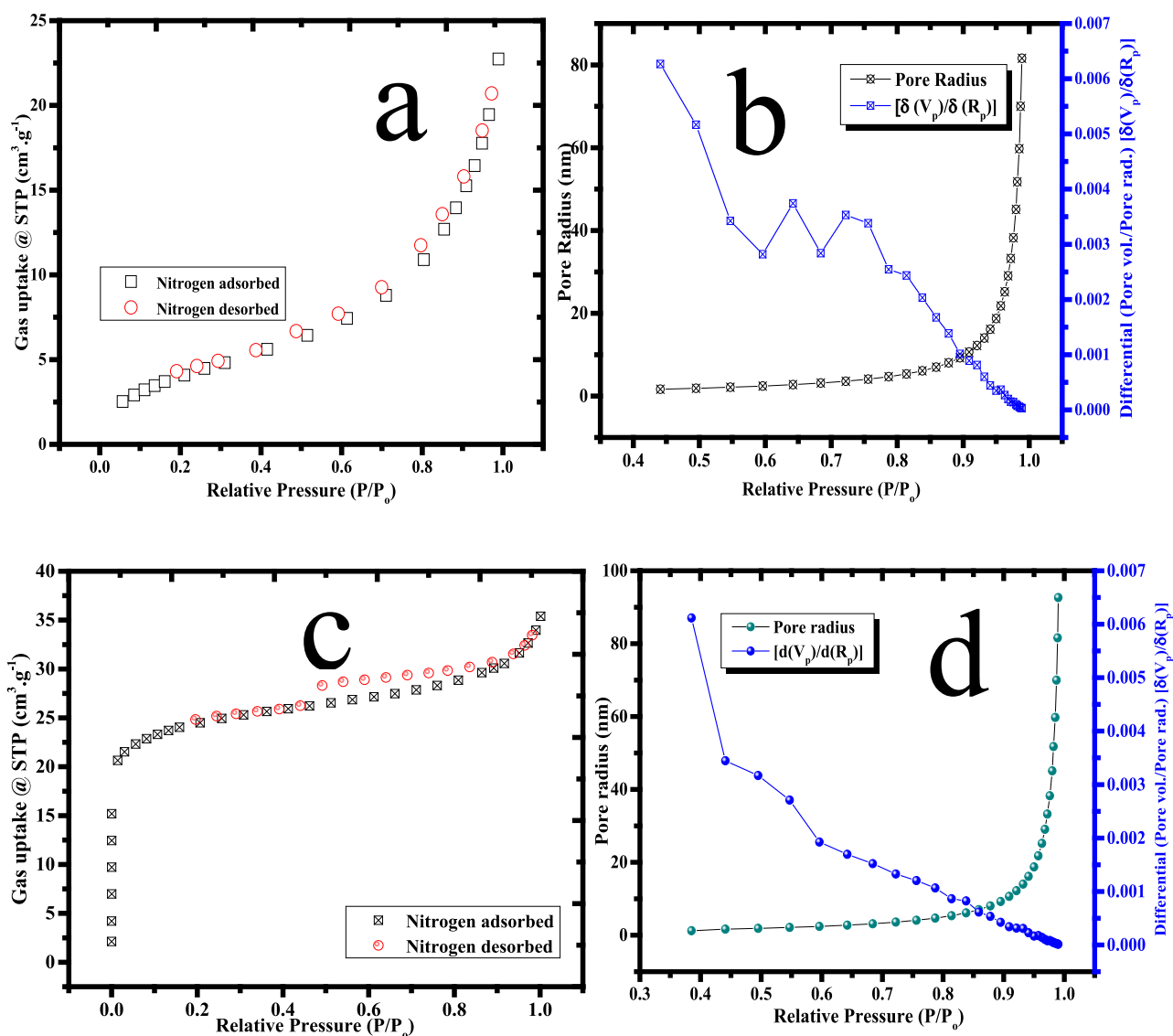


Figure 2. Plots of (a) N₂ gas uptake by SSZC (cm³·g⁻¹ STP) against relative pressure, (b) relative pressure against pore radius (nm) and the differential of pore volume/pore radius, (c) N₂ gas uptake by raw zeolite (cm³·g⁻¹ STP) against relative pressure, and (d) relative pressure against pore radii (nm) and the differential of pore volume/pore radius.

confirms that the zeolite-silica interphase's diffraction peaks clearly show the presence of both components in SSZC.⁴⁰

3.1.2. Brunauer–Emmett–Teller (BET) Physisorptometry of SSZC. The specific surface area of an adsorbent is a physical property that influences its adsorption capacity for adsorbates. Essentially, it is directly related to other fundamental physical properties of an adsorbent, such as pore width, pore volume, surface uniformity, and surface energy.⁴¹ Figure 2a–d shows the plots of N₂ gas uptake (cm³·g⁻¹ STP) against relative pressure and the plots of relative pressure against pore radius (nm), and the differential of pore volume/pore radius for SSZC and raw zeolite, respectively. The BET-specific surface area and pore volume of SSZC are 41.3 m²·g⁻¹ and 0.08 cm³·g⁻¹, respectively. The BET-specific surface area and pore volume of raw zeolite are 92 m²·g⁻¹ and 0.19 cm³·g⁻¹, respectively. Zeolites have been known as molecular sieves with particles that are less agglomerated, with good pores and increased structural stability when compared to the physicochemical properties of most materials. These properties place them in a vantage position to overcome the diffusion

limitations, which are the challenges associated with numerous molecular sieves and adsorbents during application. The ability of zeolites to overcome diffusion limitations makes them good adsorbents and support materials for adsorbents. Also, zeolites are known to enhance the surface properties of adsorbents when used as support (co-adsorbents) due to the interconnectivity of their pores.⁴²

The BET analysis revealed that the active sites containing the functional moieties and pores of SSZC were responsible for the adsorption of PMPs, such that PMPs diffused from their bulk phase into the external surface of SSZC. This depicts the liquid film/boundary layer diffusion of PMPs onto the surface of SSZC (surface diffusion). After that, the gradual migration of PMPs into the intraparticles of SSZC strongly determines the rate-limiting step of the adsorption process (intraparticle diffusion). Finally, PMPs are migrated into the active sites of SSZC via pore migration through the liquid-filled pores or solid migration mechanism (pore diffusion or solid diffusion).^{43–45}

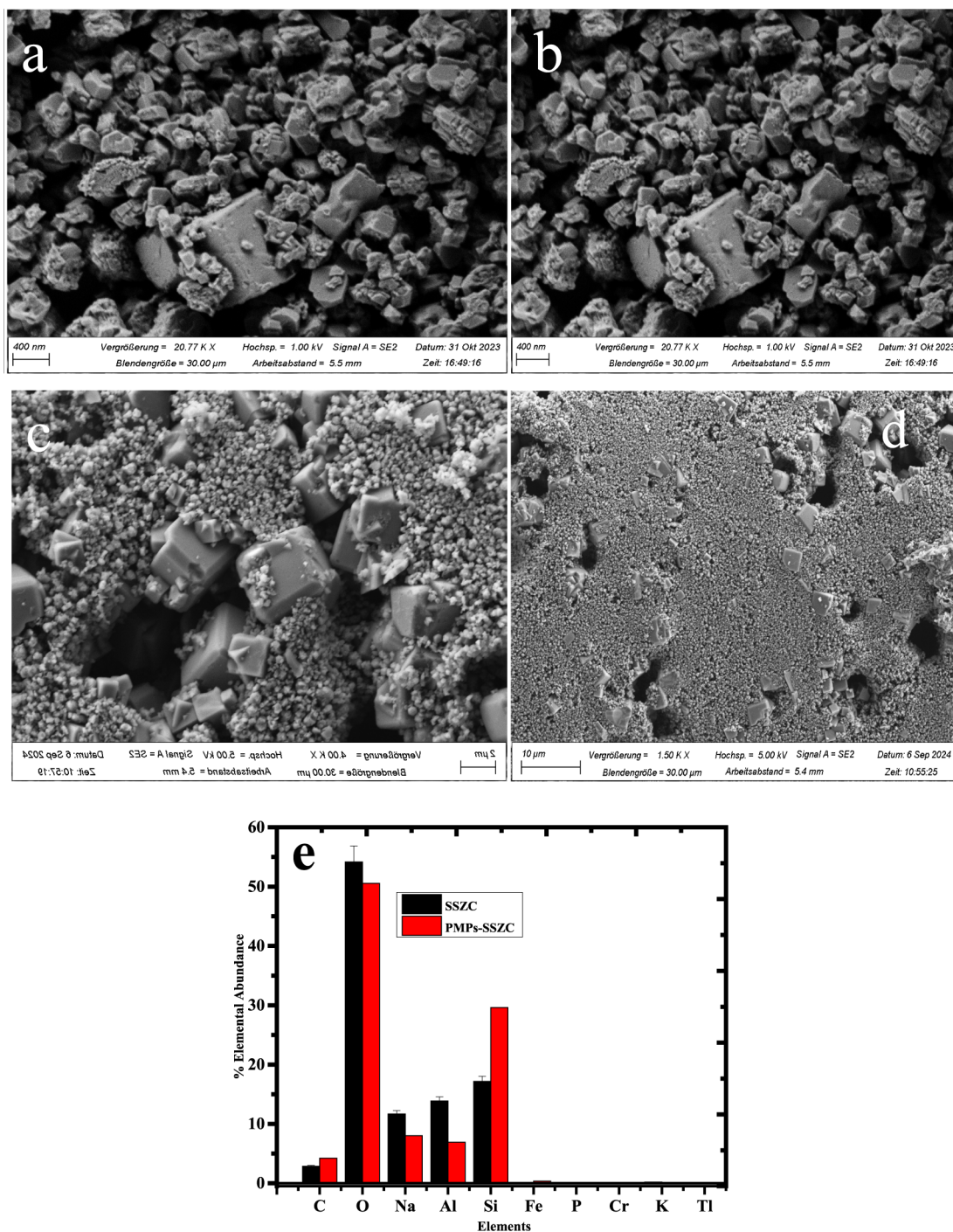


Figure 3. SEM images of SSZC at (a, b) 400 nm, PMPs-SSZC at (c) 2 μm , (d) 10 μm , and (e) EDX plot for % elemental abundance of SSZC and PMPs-SSZC.

The adsorption process is an amalgamation of one, two, or three of these diffusion mechanisms. It suffices to state that suitable pore channels and surface area present in adsorbents entrap target solutes (adsorbates) through an intragranular diffusion mechanism. This swiftly amplifies the uptake of solutes by materials (solute–materials interaction) by weak hydrophobic interactions, such as noncovalent aromatic π -system, electron donor–acceptor interactions, van der Waals forces, covalent bonding, hydrogen bonding, among others.^{43,44}

3.1.3. Scanning Electron Microscopy–Energy-Dispersive X-Ray Analysis (SEM–EDX) of SSZC. SEM is a method used for the microstructural analysis of adsorbents. It gives information about the topographic features, location of electrical defects, phase distribution, texture, variation of surface composition, morphology, and orientation.^{41,46} On the contrary, EDX is a technique used for compositional mapping and elemental identification of adsorbents.⁴¹

Figure 3a,b shows the SEM images of SSZC at different magnifications before the adsorption of PMPs onto it. These SEM images show small, clogged, and irregular cubic-like

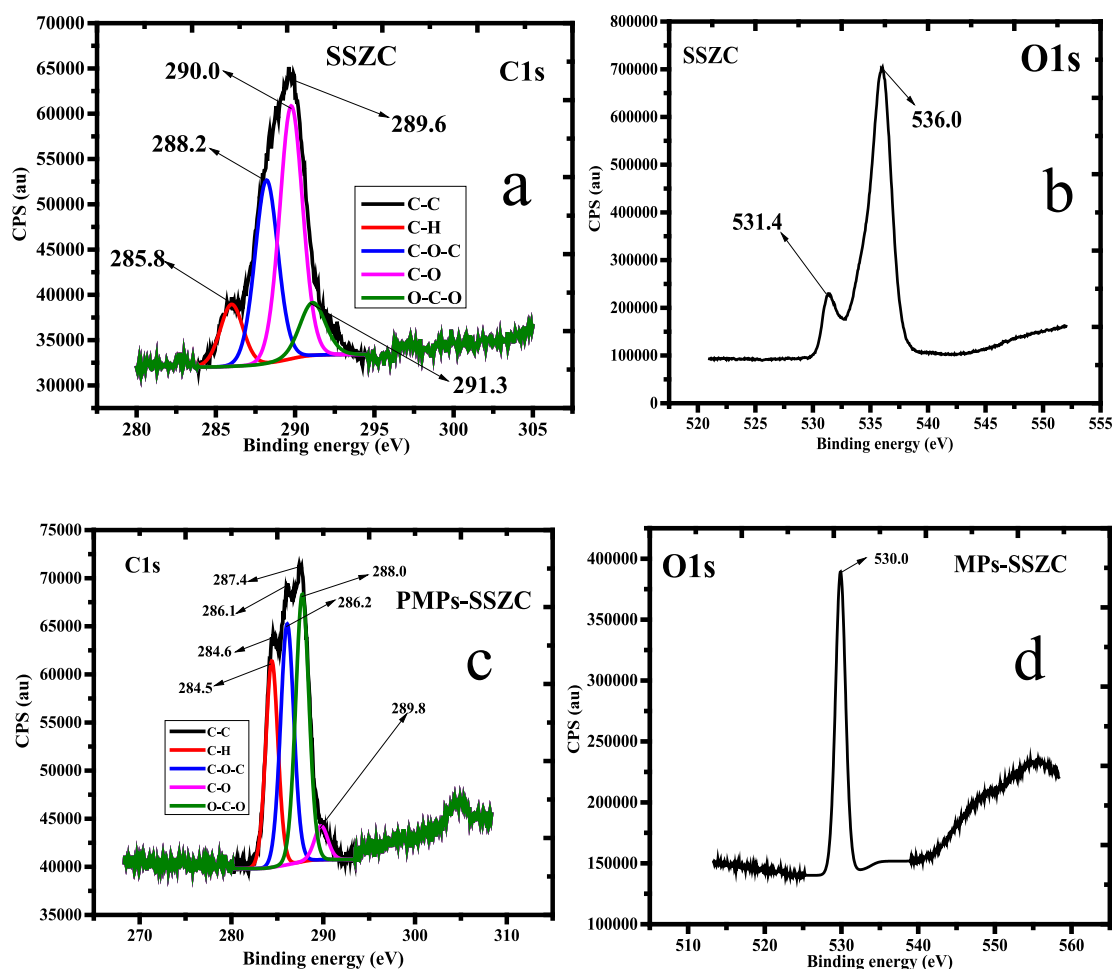


Figure 4. XPS for (a) C 1s excitation states of SSZC, O 1s excitation states of SSZC, (c) C 1s excitation states of MPs-SSZC, and (b) O 1s excitation states of MPs-SSZC.

particles that are scattered and unevenly distributed on the surface of SSZC. These clogged particles are of different sizes. After PMPs were adsorbed onto SSZC, they were observed on the surface of SSZC, as shown in Figure 3c,d. The PMP particles were seen to be distributed on the surface of SSZC after adsorption. The surface and pores of SSZC were mostly filled with PMP particles after adsorption, which supports the PMPs-SSZC hydrophobic interaction that led to the formation of hydrogen bonds between the hydrogen atoms of the styrene ring and the oxygen atoms of Al–O and Si–O–Si, as well as surface complexation reactions involving –OH, Al–O, and Si–O–Si groups in the zeolite and the carbon atoms of PMPs.^{39,47} Also, it is understood that there is the possibility of the agglomeration of PMPs on the surface and pores of SSZC, thereby filling them, as observed in Figure 3d. Figure 3e shows the elemental distribution of C, O, Na, Al, and Si in SSZC and PMPs-SSZC. The distribution of C, O, Na, Al, and Si in SSZC is 2.86%, 54.14%, 11.67%, 13.86%, and 17.16%, respectively, while the distribution in PMPs-SSZC is 4.21%, 50.56%, 8.02%, 6.92%, and 29.60%, respectively. A decrease in the distribution of C, O, and Al in PMPs-SSZC is attributed to their involvement in the formation of chemical bonds, and an increase in the distribution of C and Si in PMPs-SSZC is attributed to the formation of stable carbonyl and Al–O/Al–OH bonds.⁴⁸

3.1.4. X-Ray Photoelectron Spectroscopy (XPS) of SSZC. XPS is a surface-sensitive technique that is applied to identify atom moieties available on the surfaces of adsorbents.⁴¹ Binding energies are a function of specific delocalized electrons available on the surfaces of adsorbents for chemical interactions between adsorbents and target contaminant molecules.^{41,49} Figure 4a shows the C 1s excitation states of SSZC that comprise C–H, C–O–C, C–C, C–O, and O–C–O bonds, which were found at the binding energies of 285.8, 288.2, 289.6, 290.0, and 291.3 eV, respectively. Additionally, Figure 4b shows the O 1s excitation states of SSZC, with binding energies at 531.4 and 536.0 eV, corresponding to the O–H bond.⁴⁹ Figure 4c shows the C 1s excitation state for the adsorption of PMPs by SSZC to form C–H, C–O–C, C–C, C–O, and O–C–O bonds at 284.5, 286.2, (284.6, 286.1, 287.4), 289.8, and 288.0 eV, respectively. It was observed that after the adsorption of PMPs by SSZC, the binding energies of the C 1s excitation state decreased and two new peaks were formed for the C–C bond at 284.6 and 286.1 eV.⁵⁰ In Figure 4d, it was observed that the two peaks of O 1s excitation states of SSZC collapsed into a peak with a decrease in the binding energy to 530.0 eV after the adsorption of PMPs by SSZC. It is understood that the observed decrease of the binding energies and the formation of two new peaks for the C 1s excitation state were due to the emergence of carbonyl bonds. These carbonyl bonds were symmetric aldehyde and ketone bonds

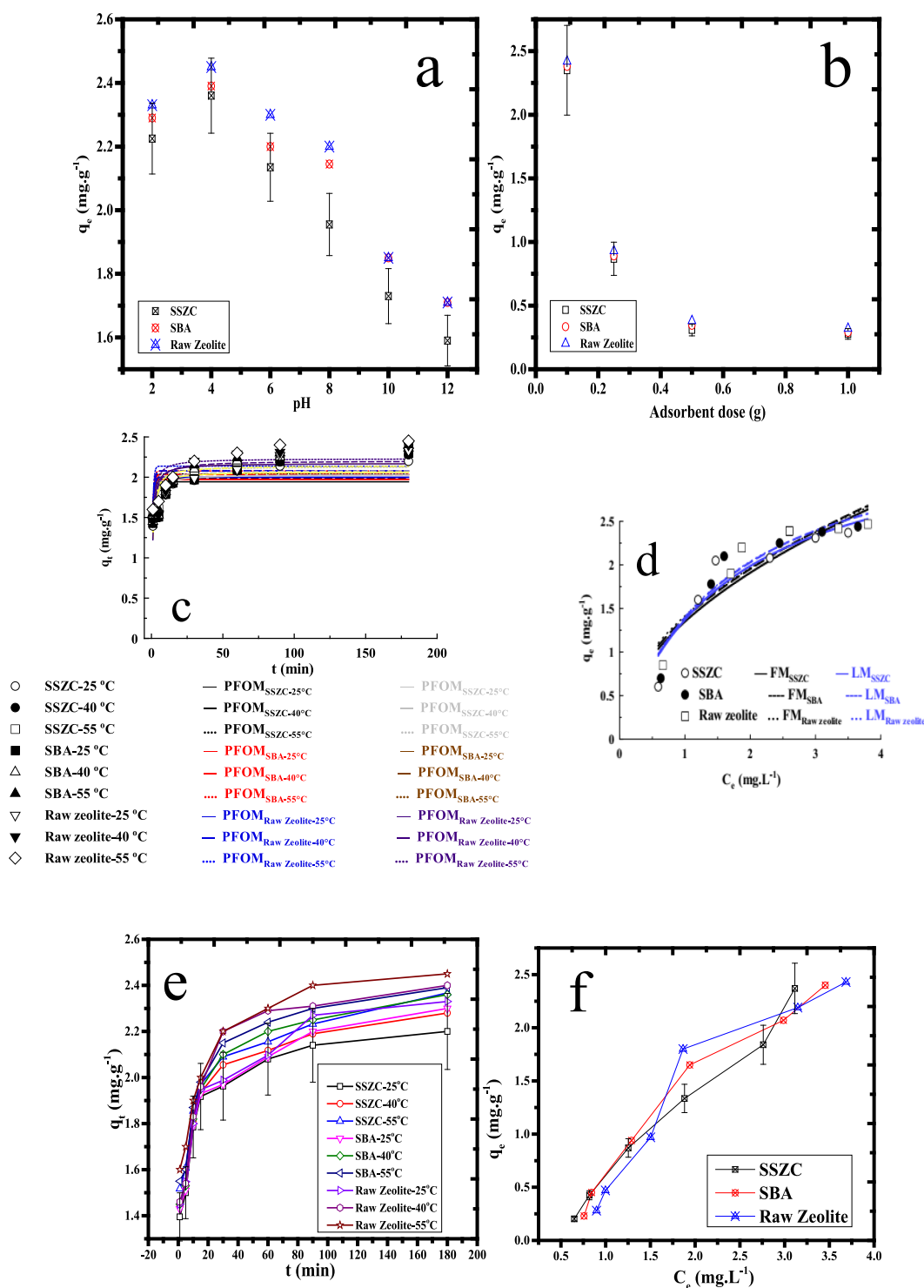


Figure 5. (a) Plot of q_e (mg·g⁻¹) against pH for the adsorption of PMPs by SSZC, SBA, and raw zeolite, and (b) plot of q_e (mg·g⁻¹) against adsorbent dose (g) for the uptake of PMPs by SSZC, SBA, and raw zeolite. (c) Nonlinear kinetic plots at different temperatures, (d) nonlinear equilibrium plots, (e) kinetic plots of q_e (mg·g⁻¹) against t (min) and (f) equilibrium plots of q_e (mg·g⁻¹) against C_e (mg·L⁻¹) for the adsorption of PMPs by SSZC, SBA, and raw zeolite.

formed from electron donor–acceptor interactions and non-covalent aromatic π -interactions between PMPs and SSZC. Additionally, the adsorption of PMPs by SSZC led to the formation of covalent bonds among methylene/methyl groups and Si–O/Al–O moieties.^{50,51} The collapse of two peaks into one, as observed in the O 1s excitation state, shows the formation of hydrogen bonds and hydrophobic interactions

that resulted from the reaction between –OH and Si–O/Al–O. The results from XPS are in tandem with that of ATR-IR, which confirms that the functional groups in SSZC were responsible for PMP adsorption.^{50–53}

3.2. Adsorption Studies. **3.2.1. Effect of pH on the Adsorption of PMPs.** Solution pH significantly influences the adsorption of adsorbates onto adsorbents. Figure 5a shows the

plot of q_e ($\text{mg}\cdot\text{g}^{-1}$) against pH for the adsorption of PMPs by SSZC, SBA, and raw zeolite. The adsorption of PMPs by SSZC, SBA, and raw zeolite increased from 2.23 to 2.36 $\text{mg}\cdot\text{g}^{-1}$ (89.2% to 94.4%), 2.29 to 2.39 $\text{mg}\cdot\text{g}^{-1}$ (91.6% to 95.6%), and 2.33 to 2.45 $\text{mg}\cdot\text{g}^{-1}$ (93.2% to 98.0%) as pH increased from 2.0 to 4.0. However, as the pH increased from 6.0 to 12.0, a decrease in the amount of PMPs adsorbed by SSZC, SBA, and raw zeolite was observed, with values dropping from 2.36 to 1.59 $\text{mg}\cdot\text{g}^{-1}$ (89.2% to 63.6%), 2.39 to 1.71 $\text{mg}\cdot\text{g}^{-1}$ (91.6% to 68.4%), and 2.45 to 1.75 $\text{mg}\cdot\text{g}^{-1}$ (98.0% to 70.0%). This trend that was observed was due to the fact that PMPs are slightly negative, and their adsorption would be favored at pH values in the acidic region electrostatic attraction and hydrophobic interaction that occurred from hydrogen bonding, van der Waal interactions, and Al–O– π , Si–O–Si– π , NH– π , and CO– π interaction. Consequently, the amounts of PMPs adsorbed by SSZC, SBA, and raw zeolite decreased as the pH shifted towards the basic region due to electrostatic repulsion. Conversely, the decrease in the amount of PMPs adsorbed by SSZC from pH 6.0 to 12.0 was due to the electrostatic repulsion between the negatively charged surfaces of SSZC, SBA, and raw zeolite and the slightly negative PMPs.^{24,25,29}

3.2.2. Effect of Adsorbent Dose on the Adsorption of PMPs. The adsorbent dose is an essential experimental variable for the determination of the adsorption capacities of materials based on their mass differential. The bulk transfer of target molecules from solution media onto the surfaces of adsorbents is a function of the diffusion length (mass transport) during adsorbate–adsorbent interactions.^{52,54} It was observed that the adsorption of PMPs by SSZC decreased from 2.35 to 0.33 $\text{mg}\cdot\text{g}^{-1}$ (94–13.2%) as the mass of SSZC increased from 0.1 to 1.0 g, respectively (Figure 5b).

The trend of this result is attributed to the clogging of SSZC as its weight increased, which led to an increase in diffusion pathways for the migration of PMPs onto the surface of SSZC. This occurrence reduced the PMP diffusion rate into the film, intraparticles, and pores of SSZC.^{44,55} Mass transport accounts for the diffusion of PMPs from the bulk solution to the SSZC particle surface, diffusion of PMPs across the boundary layer of SSZC particles, and intraparticle diffusion of PMPs from the boundary layer into the pore walls of SSZC.⁵⁵

3.2.3. Adsorption Kinetics, Thermodynamics, and Equilibrium. Adsorption kinetics provides in-depth insights into the steps that are taken into consideration before the uptake of contaminants onto adsorbents' surfaces. In this vein, the modeling and interpretation of kinetic data are suitable criteria to rate the adsorption performance. The deduction from the adsorption kinetics is a pointer to understanding its complex mechanism, feasibility of the adsorption process, and the rate-limiting steps.⁵⁶ Adsorption kinetics is the rate of mass transfer of target molecules onto the surfaces of adsorbents.^{54,55} Figure 5c shows the nonlinear kinetic plots for the adsorption of PMPs by SSZC, SBA, and raw zeolite at different temperatures. The experimental data better fit PSOM than PFOM. This means that there was a preponderance for this process to be dominated by chemisorption as the rate-limiting step. The pseudo-second-order rate constant ($\text{g}\cdot\text{mg}^{-1}\cdot\text{min}^{-1}$) increases from 0.76 to 0.91, 0.8 to 0.97 and 1.40 to 1.55 for SSZC, SBA, and raw zeolite as temperature increases from 25 to 55 °C, respectively (Table 1). This implies that the rate of adsorption of PMPs by SSZC, SBA, and raw zeolite increased at elevated temperatures. The rise in temperature increases the mobility of

Table 1. Kinetic Parameters for the Adsorption of PMPs by SSZC, SBA, and Raw Zeolites at Different Temperatures

	SSZC		
	25 °C	40 °C	55 °C
PFOM			
k_1 (min^{-1})	1.24	1.27	1.42
q_e ($\text{mg}\cdot\text{g}^{-1}$)	2.02	2.03	2.04
r^2	0.75	0.83	0.88
PSOM			
k_2 ($\text{g}\cdot\text{mg}^{-1}\cdot\text{min}^{-1}$)	0.76	0.85	0.91
q_e ($\text{mg}\cdot\text{g}^{-1}$)	2.04	2.08	2.12
r^2	0.94	0.95	0.98
	SBA		
	25 °C	40 °C	55 °C
PFOM			
k_1 (min^{-1})	1.28	1.31	1.47
q_e ($\text{mg}\cdot\text{g}^{-1}$)	2.07	2.08	2.11
r^2	0.82	0.85	0.91
PSOM			
k_2 ($\text{g}\cdot\text{mg}^{-1}\cdot\text{min}^{-1}$)	0.81	0.89	0.97
q_e ($\text{mg}\cdot\text{g}^{-1}$)	2.13	2.26	2.29
r^2	0.97	0.98	0.98
	Raw zeolite		
	25 °C	40 °C	55 °C
PFOM			
k_1 (min^{-1})	0.92	0.93	0.95
q_e ($\text{mg}\cdot\text{g}^{-1}$)	2.04	2.08	2.11
r^2	0.83	0.86	0.90
PSOM			
k_2 ($\text{g}\cdot\text{mg}^{-1}\cdot\text{min}^{-1}$)	1.40	1.44	1.55
q_e ($\text{mg}\cdot\text{g}^{-1}$)	2.17	2.23	2.35
r^2	0.97	0.98	0.99

PMPs onto the surface of SSZC, SBA, and raw zeolite. The adsorption of PMPs by SSZC, SBA, and raw zeolite for the first 60 min increased from 1.40 to 2.08 $\text{mg}\cdot\text{g}^{-1}$, 1.45 to 2.12 $\text{mg}\cdot\text{g}^{-1}$, 1.52 to 2.16 $\text{mg}\cdot\text{g}^{-1}$, 1.43 to 2.09 $\text{mg}\cdot\text{g}^{-1}$, 1.45 to 2.20 $\text{mg}\cdot\text{g}^{-1}$, 1.55 to 2.24 $\text{mg}\cdot\text{g}^{-1}$ and 1.45 to 2.10 $\text{mg}\cdot\text{g}^{-1}$, 1.46 to 2.29 $\text{mg}\cdot\text{g}^{-1}$, and 1.60 to 2.40 $\text{mg}\cdot\text{g}^{-1}$ respectively. A similar trend was observed by Babalar et al.,⁵⁷ Sajjan et al.,⁵⁸ Zhang et al.,⁴⁸ Wu et al.⁴⁷ and Yuan et al.¹⁴ After 60 min, the adsorption of PMPs by SSZC, SBA, and raw zeolite decreased due to the filling of the surfaces and pores of these adsorbents. This plays a major role in the rate at which PMPs migrate into the active sites and pores of SSZC, SBA, and raw zeolite in a rapid sequence until equilibrium was reached.^{54,55} The rate constants for PFOM and PFOM increased with an increase in temperature. This shows that the adsorption of PMPs onto SSZC, SBA, and raw zeolite was influenced by temperature rise resulting in an increase in kinetic energy of adsorption and the formation of chemical bonds.⁴⁸

Adsorption isotherms are thermodynamic equilibrium relationships among adsorbate–adsorbent interactions at constant temperatures. They establish the uptake capacities or binding interactions among the adsorbates and adsorbents. Equilibrium data generated from experiments are described by adsorption isotherms, which, in turn, give information on the interactive mechanisms of the adsorption system. The curve fitting for equilibrium data is very cogent in the analysis of the performance of adsorption processes.^{59–61} At equilibrium (initial concentrations of 1 to 10 $\text{mg}\cdot\text{L}^{-1}$), the amounts of

PMPs adsorbed by SSZC, SBA, and raw zeolite at 25 °C increased from 0.60 to 2.37 mg·g⁻¹, 0.65 to 2.40 mg·g⁻¹, and 0.78 to 2.43 mg·g⁻¹, respectively. Similar trends were observed by Zhang et al.,⁴⁸ Babalar et al.,⁵⁷ Wang et al.,⁶² Wu et al.,⁴⁷ Zhu et al.,⁶³ Zhao et al.⁶⁴ and Han et al.⁶⁵ The Langmuir isotherm better described the equilibrium data, and it revealed the Langmuir monolayer adsorption capacities, q_{mLa} , of SSZC, SBA, and raw zeolite for PMPs to be 2.41 mg·g⁻¹, 2.43 mg·g⁻¹, and 2.45 mg·g⁻¹, respectively (Figure Sd and Table 2). This shows that the adsorption of PMPs onto these adsorbents was favored by the formation of monolayer coverage rather than multilayer coverage.

Table 2. Equilibrium Parameters for the Adsorption of PMPs by SSZC, SBA, and Raw Zeolite at Various Temperatures

		SSZC		
FM	K_{Fr} (mg/g)(L/mg) ^{1/n}	1/n	r^2	
		1.99	1.35	0.90
LM	K_{La} (L·mg ⁻¹)	q_{mLa} (mg·g ⁻¹)	r^2	
		0.94	2.41	0.97
		SBA		
FM	K_{Fr} (mg/g)(L/mg) ^{1/n}	1/n	r^2	
		1.37	1.25	0.90
LM	K_{La} (L·mg ⁻¹)	q_{mLa} (mg·g ⁻¹)	r^2	
		0.81	2.43	0.97
		Raw zeolite		
FM	K_{Fr} (mg/g)(L/mg) ^{1/n}	1/n	r^2	
		1.56	1.39	0.91
LM	K_{La} (L·mg ⁻¹)	q_{mLa} (mg·g ⁻¹)	r^2	
		0.94	2.45	0.98

Wang et al.⁶² reported the q_{mLa} of PMPs adsorbed by 10 mg each of magnetic biochar (MBC), Mg-MBC, and Zn-MBC to

be 374.57, 334.03, and 355.72 mg·g⁻¹, respectively, with an initial concentration of 100 mg·L⁻¹ after 5 h at 25 °C. Singh et al.⁶⁶ reported the q_{mLa} of PMPs adsorbed by 5 mg each of *Prosopis juliflora* biochar thermally treated at 550 °C (Fe-PJB-550) and Fe-PJB-850 for carboxyl-PMPs to be 132.73 and 225.11 mg·g⁻¹ respectively, with an initial concentration of 125 mg·L⁻¹ after 30 min at 25 °C. Similarly, Singh and co-researchers⁶⁶ reported the q_{mLa} of PMPs adsorbed by 5 mg each of Fe-PJB-550 and Fe-PJB-850 for amine-PMPs to be 290.20 and 168.79 mg·g⁻¹, respectively, with an initial concentration of 125 mg·L⁻¹ after 30 min at 25 °C. According to Shi and his colleagues, the q_{mLa} of 30 mg of cetyltrimethylammonium bromide magnetic biochar for the adsorption of PMPs and carboxyl-PMPs at an initial concentration of 20 mg·L⁻¹ after 24 h at 25 °C to be 163.40 and 159.60 mg·g⁻¹, respectively.⁶⁷ Arenas et al.⁶⁸ revealed that the q_{mLa} of 5 g of granular activated charcoal for the adsorption PMPs at an initial concentration of 40 mg·L⁻¹ after 4 h at 25 °C was 2.15 mg·g⁻¹. Babalar et al.⁵⁷ revealed in their research findings that 10 mg each of activated biochar (AB), magnetic-activated biochar-zeolite (MABZ), and polyethylene glycol/polyethylenimine-coated MABZ has q_{mLa} of 454.50, 526.31, and 736.0 mg·g⁻¹ at an initial concentration of 100 mg·L⁻¹ after 4 h at 25 °C, respectively. Heo et al.²⁴ revealed in their research that 20 mg of magnetic magnetite (Fe₃O₄) has q_{mLa} of 2,799.2 mg·g⁻¹ at an initial concentration of 300 mg·L⁻¹ after 3 h at 25 °C. Zhang and his colleagues⁴⁸ discovered that 5 g of London plane bark biochar has q_{mLa} of 71.90 mg·g⁻¹ at an initial concentration of 300 mg·L⁻¹ after 3 h at 25 °C. Figure 5e,f shows the kinetic plots of q_t (mg·g⁻¹) against t (min) and the equilibrium plots of q_e (mg·g⁻¹) against C_e (mg·L⁻¹) for the adsorption of PMPs by SSZC, SBA, and raw zeolite, respectively.

A comprehensive comparison of these research findings in the literature with our research findings shows that most

Table 3. Adsorption Capacities of Certain Materials for the Removal of PMPs^{70a}

S/No.	Adsorbents	q_{mLa} (mg g ⁻¹)	Conditions	Ref.
1	Mg/Zn-modified biochar	374.57	pH = —, $T = 25$ °C, IC = 300 mg·L ⁻¹ , AD = 100 mg	62
2	Chitin sponge materials	5.44	pH = 7.0, $T = 25$ °C, IC = 20 mg·L ⁻¹ , AD = 10 mg	71
3	Graphene/layer double oxide	209.39	pH = 9.0, $T = 25$ °C, IC = 400 mg·L ⁻¹ , AD = 250 mg	12
4	Magnetic ZIF-8	24.50	pH = —, $T = 25$ °C, IC = 25 mg·L ⁻¹ , AD = 5 mg	11
5	Fly ash magnetic material	89.90	pH = 7.0, $T = 25$ °C, IC = 30 mg·L ⁻¹ , AD = 20 mg	72
6	Chitin/graphene oxide sponge	5.90	pH = 6.0, $T = 25$ °C, IC = 15 mg·L ⁻¹ , AD = 10 mg	13
7	Aquifer fine sand	0.00857	pH = 7.0, $T = 25$ °C, IC = 10 mg·L ⁻¹ , AD = 2 g	73
8	Reduced graphene oxide	617.28	pH = 6.0, $T = 26$ °C, IC = 600 mg·L ⁻¹ , AD = 1.5 mg	14
9	Magnetic iron oxide	2,799.20	pH = 3.0, $T = 25$ °C, IC = 300 mg·L ⁻¹ , AD = 100 mg	24
10	Cr-MOF	319.49	pH = 5.0, $T = 25$ °C, IC = 70 mg·L ⁻¹ , AD = 4 mg	10
11	Co/Mn-Kaolin	22.00	pH = —, $T = 25$ °C, IC = 100 mg·L ⁻¹ , AD = 10 mg	74
12	Fe-Kaolin	13.68	pH = —, $T = 25$ °C, IC = 100 mg·L ⁻¹ , AD = 10 mg	74
13	Fe ₃ O ₄ nanoparticles	7.9	pH = 6.5, $T = 25$ °C, IC = 60 mg·L ⁻¹ , AD = 60 mg	15
14	Sugar cane bagasse biochar	44.9	pH = —, $T = 25$ °C, IC = 10 mg·L ⁻¹ , AD = 15 mg	75
15	Granular activated carbon	2.2	pH = 7.4, $T = 25$ °C, IC = 40 mg·L ⁻¹ , AD = 5 g	68
16	Amino-functionalized zeolite series/H ₃ PO ₄ -biochar	4.85	pH = 7.0, $T = 25$ °C, IC = 10 mg·L ⁻¹ , AD = 50 mg	70
17	London plane bark biochar	71.90	pH = 5.0, $T = 24$ °C, IC = 500 mg·L ⁻¹ , AD = 5 g	48
18	Corn-cob-derived mesoporous biochar	56.02	pH = —, $T = 25$ °C, IC = 50 mg·L ⁻¹ , AD = 100 mg	63
19	Magnetic rice husks biochar	39.87	pH = 6.0–7.0, $T = 25$ °C, IC = 60 mg·L ⁻¹ , AD = 10 mg	47
20	SSZC	2.41	pH = 4.0, $T = 25$ °C, IC = 10 mg·L ⁻¹ , AD = 100 mg	This study

^aIC: Initial concentration, AD: Adsorbent dosage.

research works were done with initial concentrations higher than the initial concentration that we used for our studies (Table 3). In pragmatic terms, these high concentrations do not depict a true representation of environmental microplastics contamination levels. However, the research findings of Singh et al.⁶⁶ show a rapid removal of PMPs, with equilibrium achieved within 30 min. An observable limitation of most adsorbents in the literature is that their synthesis routes tend to be either expensive or energy-consuming. This shows that the design and synthesis of adsorbents for PMPs should be engineered to favor their rapid removal. This implies that during water and wastewater treatment, energy cost will be minimized, and the volume of water and wastewater that will be treated will increase. On the contrary, this will lead to the optimization of the process design and process engineering of these adsorbents on a large scale.

The thermodynamic data revealed that the adsorption of PMPs by SSZC, SBA, and raw zeolite was endothermic ($\Delta H^\circ = +2.3, +3.5, \text{ and } 5.6 \text{ kJ}\cdot\text{mol}^{-1}$), respectively, with a decrease in the degree of randomness/chaos ($\Delta S^\circ = -2.3, -4.1, \text{ and } -5.5 \text{ J}\cdot\text{mol}^{-1}\cdot\text{K}^{-1}$) and nonspontaneous ($\Delta G^\circ = +3.33 \text{ to } 3.43, +3.81 \text{ to } 4.22, \text{ and } +4.39 \text{ to } 4.88 \text{ kJ}\cdot\text{mol}^{-1}$), respectively, from 25 to 55 °C (Table 4). These thermodynamic findings reveal that certain energy barrier or adsorption energy (endothermic-based reaction) was overcome before the process could be achieved.⁶⁹

Table 4. Thermodynamic Parameters for the Adsorption of PMPs by SSZC, SBA, and Raw Zeolite at Various Temperatures

	298 K	313 K	328 K
	SSZC		
ΔG° (kJ·mol ⁻¹)	+3.33	+3.38	+3.43
ΔH° (kJ·mol ⁻¹)	+2.3		
ΔS° (J·mol ⁻¹ ·K ⁻¹)	-2.3		
	SBA		
ΔG° (kJ·mol ⁻¹)	+3.81	+4.07	+4.22
ΔH° (kJ·mol ⁻¹)	+3.5		
ΔS° (J·mol ⁻¹ ·K ⁻¹)	-4.1		
	Raw zeolite		
ΔG° (kJ·mol ⁻¹)	+4.39	+4.61	+4.88
ΔH° (kJ·mol ⁻¹)	+5.6		
ΔS° (J·mol ⁻¹ ·K ⁻¹)	-5.5		

3.2.4. Recycling Study. A recycling study is essential for the sustainability, benignity, and cost-effectiveness of producing adsorbents. Figure 6a shows a recycling study of PMP-loaded SSZC in five cycles. This study reveals that SSZC achieved 71 to 97%, 63 to 93%, 55 to 85%, and 46 to 67.5% for the removal of PMPs in ethanol, deionized water, 0.1 M nitric acid, and acetone during the first to fifth cycles, respectively. This implies that SSZC has a promising recovery potential for removing PMPs in ethanol, deionized water, and 0.1 M nitric acid, except in acetone. The recyclability of some of these solvents for SSZC is not very high, probably because PMPs are held by chemisorption onto the surface of SSZC via hydrophobic interactions, such as π - π aromatic stacking and electron donor-acceptor interactions, among others.

3.2.5. Adsorption of PMPs from Drinking Water (DGW) and Wastewater (WEW) Samples. Outside laboratory applications, SSZC was used to remove PMPs from DGW and WEW samples (see Table 5 for physicochemical properties

of WEW). The quantity of PMPs in WEW samples adsorbed by SSZC increased from 51% to 79% for 1–10 mg·L⁻¹, respectively. A similar trend was observed for the quantity of PMPs in DGW adsorbed by SSZC, which increased from 78% to 94.3% for 1–10 mg·L⁻¹, respectively (Figure 6b). The PMP molecules removed by SSZC were higher in DGW than WEW. This is simply due to the presence of a complex matrix of various contaminants present in WEW. Consequently, more contaminants present in WEW were adsorbed on the active sites of SSZC apart from PMPs.

3.2.6. Possible Mechanism for the Adsorption of PMPs by SSZC. The BET physisorption of SSZC showed that its surface comprises pores that entrapped, entangled, captured, and retained PMPs (retention mechanism). These pores on the surface of SSZC function as a molecular sieve for PMPs. The bulk diffusion of PMPs onto the pores of SSZC's surface was mechanically unhindered, and this facilitated the rapid adsorption of PMPs. It is understood that PMPs are slightly negative,^{17,76} and their adsorption by SSZC is favored at pH values in the acid region via electrostatic attraction.

There is a possibility that intermolecular interactions took place during the adsorption of PMPs onto SSZC, due to the interactions between PMPs and the O–H moiety of the O 1s excitation states of SSZC, as well as with the C–H, C–O–C, C–C, C–O, and O–C–O moieties observed in the 1s excitation states of SSZC from the XPS spectrum. The ATR-IR spectrum revealed the possible formation of hydrogen bonding, weak hydrophobic interactions, and electron donor-acceptor interactions during the adsorption of PMPs onto SSZC's surface. The rich nucleophilic centers of PMPs could serve as electron donors during their chemical interaction with the silanol moiety (electron acceptor) of SSZC, leading to the formation of π - π interactions. From the thermodynamic standpoint, the mechanism of adsorption of PMPs by SSZC could be chemisorptive due to the energy requirement for the formation of chemical bonds between PMPs and SSZC.^{47,70}

3.2.7. The Sustainability of the Adsorption Process on a Large Scale. The sustainability of the adsorption process on a large scale is a function of the pragmatic understanding of the performance indices (uptake capacities) of various adsorbents. These performance indices are based on their applications for the removal of target contaminants from water and wastewater (complex water matrices), considering low-cost factors, cycle assessment, and optimization of experimental variables to meet industrial conditions. Additionally, they integrate multiple perspectives to harness and standardize tunability, surface engineering, and ease of modification to suit target applications.⁷⁷ The global shortage of potable water is a very serious challenge that needs urgent attention. Attempts to solve this issue have led researchers and scientists to search for effective methods and techniques to develop adsorbents with good uptake capacities for water contaminants. Over the years, literature has shown that myriads of adsorbents synthesized by researchers and scientists possess excellent surface properties (such as high porosity, large pore volume, large surface area, and high adsorption capacity), but these adsorbents are expensive, laborious (difficult to synthesize or produce), possess low mechanical stability, have low selectivity for contaminants and are challenging to regenerate. The sustainability and large-scale applicability of adsorbents depend on their possession of good surface properties and the ease of the re-engineering of these surfaces to suit selective

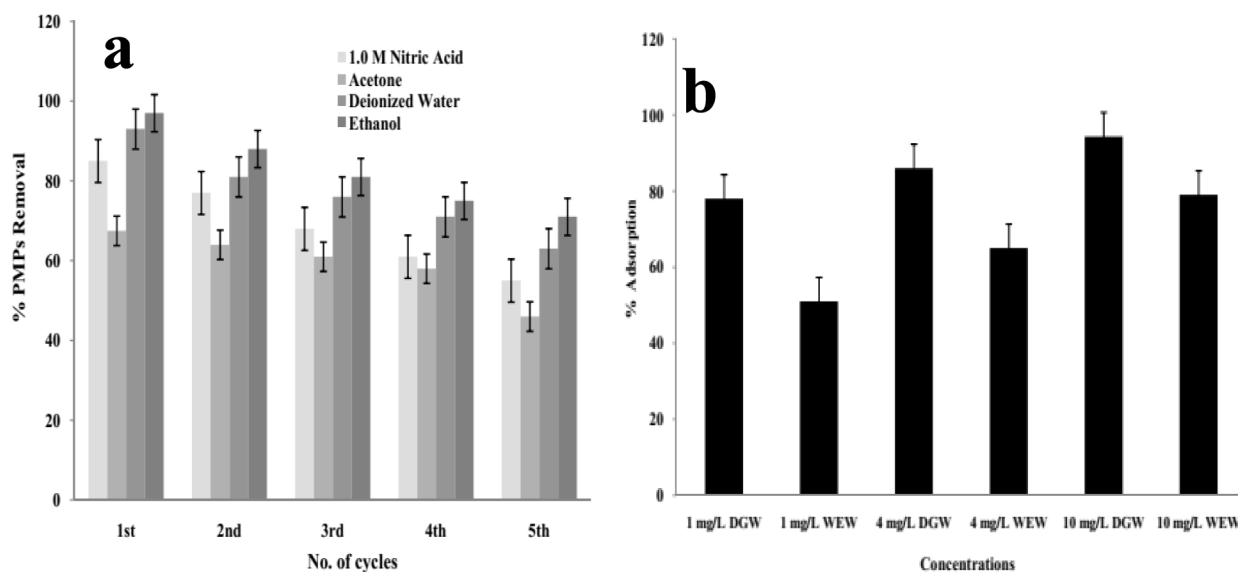


Figure 6. (a) Plots of % PMP removal from SSZC by various desorbents against various cycles and (b) % removal of PMPs in DGW and WEW by SSZC.

Table 5. Physicochemical Characterization of Wastewater

BOD ₅ (mg L ⁻¹)	COD (mg L ⁻¹)	TDS (mg L ⁻¹)	Electrical Conductivity ($\mu\text{S cm}^{-1}$)	TSS (mg L ⁻¹)	Turbidity (NTU)
282	745	793	1,462 at 11.2 °C	245	27.6

applications. This study explored adsorbents that possess certain desirable surface properties, such as ease of regeneration, benignity, facile, cost-effectiveness, and high mechanical stability. The possession of these desirable properties and the application of SSZC for the effective removal of PMPs in water and wastewater is a testament that this adsorption process is sustainable on a large scale.^{78,79} Table 3 shows the adsorption capacities of various materials for PMPs.

4. CONCLUSION

The potential of facile and benign SSZC was studied for the removal of polystyrene microplastics (PMPs) in water. Surface characterization of SSZC by zeta potential, ATR-IR, SEM-EDX, TGA, DTG, XRD, BET,²⁷ Al and ²⁹Si MAS NMR, and XPS showed that some functional moieties such as aromatic olefin, amine, hydroxyl, carbonyl, carboxyl, siloxane, and silanol were responsible for the adsorption of PMPs by SSZC. Data analysis revealed that Langmuir and pseudo-second-order models better fit the experimental data, with the Langmuir monolayer coverage capacity ($q_{m,a}$) of SSZC being 2.41 mg·g⁻¹ of PMPs. In this study, SSZC demonstrated potential for treating water contaminated with PMPs.

■ ASSOCIATED CONTENT

SI Supporting Information

The Supporting Information is available free of charge at <https://pubs.acs.org/doi/10.1021/acsestwater.4c00558>.

Zeta potential (ZP); thermogravimetry (TG) and differential thermogravimetry (DTG); attenuated total reflectance-infrared (ATR-IR) spectrophotometry; and

²⁷Al and ²⁹Si solid-state magic angle spinning-nuclear magnetic resonance (MAS-NMR) (PDF)

■ AUTHOR INFORMATION

Corresponding Author

Martins O. Omorogie – Chair of Urban Water Systems Engineering, School of Engineering and Design, Technical University of Munich, Garching 85748, Germany; Department of Chemical Sciences, Faculty of Natural Sciences and Environmental Science and Technology Research Unit, African Centre of Excellence for Water and Environmental Research (ACEWATER), Redeemer's University, Ede 232101, Nigeria; orcid.org/0000-0001-9697-2960; Email: mo.omorogie@tum.de, omorogiem@run.edu.ng, dromorogiemoon@gmail.com

Author

Brigitte Helmreich – Chair of Urban Water Systems Engineering, School of Engineering and Design, Technical University of Munich, Garching 85748, Germany; orcid.org/0000-0003-4224-3329

Complete contact information is available at:

<https://pubs.acs.org/doi/10.1021/acsestwater.4c00558>

Author Contributions

M.O.O.: Conceptualization; Data Curation; Formal Analysis; Funding acquisition; Investigation; Methodology; Project administration; Resources; Software; Supervision; Validation; Visualization; Writing—original draft; Writing—review and editing; B.H.: Formal Analysis; Funding acquisition; Investigation; Methodology; Project administration; Resources; Software; Supervision; Validation; Visualization; Writing—original draft; Writing—review and editing. CRediT: **Martins O. Omorogie** conceptualization, data curation, formal analysis, funding acquisition, investigation, methodology, project administration, resources, software, validation, visualization, writing - original draft, writing - review & editing; **Brigitte Helmreich** funding acquisition, project administration, supervision, validation, writing - original draft, writing - review & editing.

Notes

The authors declare no competing financial interest.

ACKNOWLEDGMENTS

Dr Martins O. Omorogie and Prof. Dr Brigitte Helmreich are immensely grateful to the Alexander von Humboldt Foundation, Germany, and the Carl Friedrich von Siemens Foundation, Germany, for the award of Research Fellowship for Experienced Researcher to Dr Martins O. Omorogie (NGA-1201082-HFST-E).

REFERENCES

- (1) PlasticEuropePlastics—the facts 2020PlasticEurope202011–64
- (2) Fu, X.; Zhang, S.; Zhang, X.; Zhang, Y.; Li, B.; Jin, K.; Feng, X.; Hong, J.; Huang, X.; Cao, H.; et al. Sustainable Microplastic Remediation with Record Capacity Unleashed via Surface Engineering of Natural Fungal Mycelium Framework. *Adv. Funct. Mater.* **2023**, *33*, 2212570.
- (3) Gomez-Gonzalez, M. A.; Da Silva-Ferreira, T.; Clark, N.; Clough, R.; Quinn, P. D.; Parker, J. E. Toward Understanding the Environmental Risks of Combined Microplastics/Nanomaterials Exposures: Unveiling ZnO Transformations after Adsorption onto Polystyrene Microplastics in Environmental Solutions. *Global Challenges* **2023**, *7*, 2300036.
- (4) John, K. I.; Omorogie, M. O.; Adeleye, A. T.; Bayode, A. A.; Helmreich, B. Environmental Microplastics Distribution, Impact, and Determination Methods: a Review. *J. Anal. Chem.* **2023**, *78*, 1199–1212.
- (5) John, K. I.; Omorogie, M. O.; Bayode, A. A.; Adeleye, A. T.; Helmreich, B. Environmental microplastics and their additives—a critical review on advanced oxidative techniques for their removal. *Chem. Pap.* **2023**, *77*, 657–676.
- (6) PlasticEurope. *Plastics—the facts 2020: An Analysis Of European Plastics Production, Demand And Waste data*, (22 January 2021), PlasticEurope, 2020.
- (7) Lin, P.-Y.; Wu, I.-H.; Tsai, C.-Y.; Kirankumar, R.; Hsieh, S. Detecting the release of plastic particles in packaged drinking water under simulated light irradiation using surface-enhanced Raman spectroscopy. *Anal. Chim. Acta* **2022**, *1198*, 339516.
- (8) Steinmetz, Z.; Kintzi, A.; Muñoz, K.; Schaumann, G. E. A simple method for the selective quantification of polyethylene, polypropylene, and polystyrene plastic debris in soil by pyrolysis-gas chromatography/mass spectrometry. *J. Anal. Appl. Pyrolysis* **2020**, *147*, 104803.
- (9) Yang, M.; Zhang, B.; Chen, X.; Kang, Q.; Gao, B.; Lee, K.; Chen, B. Transport of Microplastic and Dispersed Oil Co-contaminants in the Marine Environment. *Environ. Sci. Technol.* **2023**, *57*, S633–S645.
- (10) Modak, S.; Kasula, M.; Esfahani, M. R. Nanoplastics removal from water using metal–organic framework: investigation of adsorption mechanisms, kinetics, and effective environmental parameters. *ACS Appl. Eng. Mater.* **2023**, *1*, 744–755.
- (11) Pasanen, F.; Fuller, R. O.; Maya, F. Fast and simultaneous removal of microplastics and plastic-derived endocrine disruptors using a magnetic ZIF-8 nanocomposite. *Chem. Eng. J.* **2023**, *455*, 140405.
- (12) Peng, G.; Xiang, M.; Wang, W.; Su, Z.; Liu, H.; Mao, Y.; Chen, Y.; Zhang, P. Engineering 3D graphene-like carbon-assembled layered double oxide for efficient microplastic removal in a wide pH range. *J. Hazard. Mater.* **2022**, *433*, 128672.
- (13) Sun, C.; Wang, Z.; Chen, L.; Li, F. Fabrication of robust and compressive chitin and graphene oxide sponges for removal of microplastics with different functional groups. *Chem. Eng. J.* **2020**, *393*, 124796.
- (14) Yuan, F.; Yue, L.; Zhao, H.; Wu, H. Study on the adsorption of polystyrene microplastics by three-dimensional reduced graphene oxide. *Water Sci. Technol.* **2020**, *81*, 2163–2175.
- (15) Zandieh, M.; Liu, J. Removal and degradation of microplastics using the magnetic and nanozyme activities of bare iron oxide nanoaggregates. *Angew. Chem., Int. Ed.* **2022**, *61*, No. e202212013.
- (16) Tang, Y.; Zhang, S.; Su, Y.; Wu, D.; Zhao, Y.; Xie, B. Removal of microplastics from aqueous solutions by magnetic carbon nanotubes. *Chem. Eng. J.* **2021**, *406*, 126804.
- (17) Shen, M.; Hu, T.; Huang, W.; Song, B.; Zeng, G.; Zhang, Y. Removal of microplastics from wastewater with aluminosilicate filter media and their surfactant-modified products: Performance, mechanism and utilization. *Chem. Eng. J.* **2021**, *421*, 129918.
- (18) Nabi, I.; Bacha, A.-U.-R.; Ahmad, F.; Zhang, L. Application of titanium dioxide for the photocatalytic degradation of macro-and micro-plastics: A review. *J. Environ. Chem. Eng.* **2021**, *9*, 105964.
- (19) Ebrahimbabaie, P.; Yousefi, K.; Pichtel, J. Photocatalytic and biological technologies for elimination of microplastics in water: Current status. *Sci. Total Environ.* **2022**, *806*, 150603.
- (20) Miri, S.; Saini, R.; Davoodi, S. M.; Pulicharla, R.; Brar, S. K.; Magdoui, S. Biodegradation of microplastics: Better late than never. *Chemosphere* **2022**, *286*, 131670.
- (21) Tang, W.; Li, H.; Fei, L.; Wei, B.; Zhou, T.; Zhang, H. The removal of microplastics from water by coagulation: A comprehensive review. *Sci. Total Environ.* **2022**, *851*, 158224.
- (22) Malankowska, M.; Echaide-Gorritz, C.; Coronas, J. Microplastics in marine environment: a review on sources, classification, and potential remediation by membrane technology. *Environ. Sci.: water Res. Technol.* **2021**, *7*, 243–258.
- (23) Nabi, I.; Bacha, A.-U.-R.; Zhang, L. A review on microplastics separation techniques from environmental media. *J. Cleaner Prod.* **2022**, *337*, 130458.
- (24) Heo, Y.; Lee, E.-H.; Lee, S.-W. Adsorptive removal of micron-sized polystyrene particles using magnetic iron oxide nanoparticles. *Chemosphere* **2022**, *307*, 135672.
- (25) Chen, Z.; Fang, J.; Wei, W.; Ngo, H. H.; Guo, W.; Ni, B.-J. Emerging adsorbents for micro/nanoplastics removal from contaminated water: Advances and perspectives. *J. Cleaner Prod.* **2022**, *371*, 133676.
- (26) Guisnet, M.; Gilson, J.-P. *Zeolites for cleaner technologies*; Imperial College Press London, 2002; Vol. 3.
- (27) Hu, G.; Yang, J.; Duan, X.; Farnood, R.; Yang, C.; Yang, J.; Liu, W.; Liu, Q. Recent developments and challenges in zeolite-based composite photocatalysts for environmental applications. *Chem. Eng. J.* **2021**, *417*, 129209.
- (28) Munir, N.; Javaid, A.; Abideen, Z.; Duarte, B.; Jarar, H.; El-Keblawy, A.; Sheteiwy, M. S. The potential of zeolite nanocomposites in removing microplastics, ammonia, and trace metals from wastewater and their role in phytoremediation. *Environ. Sci. Pollut. Res.* **2024**, *31*, 1695–1718.
- (29) Li, Y.; Zhang, S.; Liu, S.; Chen, Y.; Luo, M.; Li, J.; Xu, S.; Hou, X. Eco-friendly hydrophobic ZIF-8/sodium alginate monolithic adsorbent: An efficient trap for microplastics in the aqueous environment. *J. Colloid Interface Sci.* **2024**, *661*, 259–270.
- (30) Kulawong, S.; Chanlek, N.; Osakoo, N. Facile synthesis of hierarchical structure of NaY zeolite using silica from cogon grass for acid blue 185 removal from water. *J. Environ. Chem. Eng.* **2020**, *8*, 104114.
- (31) Yan, N.; Duan, L.-H.; He, M.; Luo, W.; Ou, Z.; Wang, J. Metal ion-supported mesoporous silica materials for the removal of sulfamethizole from water. *New J. Chem.* **2024**, *48*, 13038–13047.
- (32) Omorogie, M. O.; Ilesanmi, F. O.; Alfred, M. O.; Helmreich, B. Thermally-treated MgO/nanocrystalline cellulose immobilized onto a Santa Barbara-16 mesoporous SiO₂ template for the sequestration of antibiotics from polluted water. *New J. Chem.* **2022**, *46*, 20918–20931.
- (33) Umpleby Ii, R. J.; Baxter, S. C.; Bode, M.; Berch, J. J. K.; Shah, R. N.; Shimizu, K. D. Application of the Freundlich adsorption isotherm in the characterization of molecularly imprinted polymers. *Anal. Chim. Acta* **2001**, *435*, 35–42.
- (34) Langmuir, I. The adsorption of gases on plane surfaces of glass, mica and platinum. *J. Am. Chem. Soc.* **1918**, *40*, 1361–1403.

- (35) Lagergren, S. About the theory of so-called adsorption of soluble substances. *K. Sven. Vetenskapsakad. Handl.* **1898**, *24*, 1–39.
- (36) Ho, Y. S.; McKay, G. The kinetics of sorption of divalent metal ions onto sphagnum moss peat. *Water Res.* **2000**, *34*, 735–742.
- (37) Omorogie, M. O.; Babalola, J. O.; Unuabonah, E. I.; Gong, J. R. Kinetics and thermodynamics of heavy metal ions sequestration onto novel *Nauclea diderrichii* seed biomass. *Bioresour. Technol.* **2012**, *118*, 576–579.
- (38) Raja, P. B.; Munusamy, K. R.; Perumal, V.; Ibrahim, M. N. M. Characterization of nanomaterial used in nanobioremediation. In *Nano-bioremediation: fundamentals and applications*; Elsevier, 2022, pp. 57–83.
- (39) Ghazimoradi, M.; Soltanali, S.; Safari, N.; Ghassabzadeh, H. Synthesis of fluorinated ZSM-5 catalysts: fluoride effect on structure properties and coke resistance in n-hexane catalytic cracking. *J. Mater. Sci.* **2023**, *58*, 11551–11567.
- (40) Akti, F. Silver and zirconium mono-and bi-metallic silica mesoporous functionalized PDA materials as highly efficient reusable catalyst for reduction of 4-NP to 4-AP. *Mater. Chem. Phys.* **2023**, *304*, 127858.
- (41) Pellenz, L.; de Oliveira, C. R. S.; da Silva, A. H., Jr.; da Silva, L. J. S.; da Silva, L.; de Souza, A. A. U.; Ulson, S. M. D. A. G.; Borba, F. H.; da Silva, A. A comprehensive guide for characterization of adsorbent materials. *Sep. Purif. Technol.* **2023**, *305*, 122435.
- (42) Khatrin, I.; Abdullah, I.; McCue, A. J.; Krisnandi, Y. K. Mesoporous configuration effects on the physicochemical features of hierarchical ZSM-5 supported cobalt oxide as catalysts in methane partial oxidation. *Microporous Mesoporous Mater.* **2024**, *365*, 112896.
- (43) Gerente, C.; Lee, V.; Cloirec, P. L.; McKay, G. Application of chitosan for the removal of metals from wastewaters by adsorption—mechanisms and models review. *Crit. Rev. Environ. Sci. Technol.* **2007**, *37*, 41–127.
- (44) Önal, Y.; Akmil-Başar, C.; Sarıci-Özdemir, Ç. Investigation kinetics mechanisms of adsorption malachite green onto activated carbon. *J. Hazard. Mater.* **2007**, *146*, 194–203.
- (45) Omorogie, M. O.; Naidoo, E. B.; Ofomaja, A. E. Response surface methodology, central composite design, process methodology and characterization of pyrolyzed KOH pretreated environmental biomass: mathematical modelling and optimization approach. *Model. Earth Syst. Environ.* **2017**, *3*, 1171–1186.
- (46) Seraphin, S.; Hernandez, S.; Chandler, G.; Bentley, D.; Dorame, K.; Sellers, M. Remote Microscopy for Education and Outreach. *Microsc. Today* **2009**, *17*, 22–25.
- (47) Wu, J.; Yang, C.; Zhao, H.; Shi, J.; Liu, Z.; Li, C.; Song, F. Efficient removal of microplastics from aqueous solution by a novel magnetic biochar: performance, mechanism, and reusability. *Environ. Sci. Pollut. Res.* **2023**, *30*, 26914–26928.
- (48) Zhang, X.; Lv, D.; Liu, Z.; Xu, D.; Yang, F.; Wang, X.; Tan, Z.; Gao, W.; Liu, R.; Su, C. Removal of polystyrene microplastic from aqueous solutions with London Plane bark biochar: Pyrolysis temperature, performance and mechanism. *Colloids Surf, A* **2024**, *694*, 134159.
- (49) Xu, J.; Guo, Y.; Tang, C.; Qian, Y.; Guo, C.; Wang, Z.; Li, L. Hardwood vessel-inspired chitosan-based sponge with superior compressibility, superfast adsorption and remarkable recyclability for microplastics removal in water. *Chem. Eng. J.* **2023**, *475*, 146130.
- (50) Fu, Q.; Tan, X.; Ye, S.; Ma, L.; Gu, Y.; Zhang, P.; Chen, Q.; Yang, Y.; Tang, Y. Mechanism analysis of heavy metal lead captured by natural-aged microplastics. *Chemosphere* **2021**, *270*, 128624.
- (51) Melo-Agustín, P.; Kozak, E. R.; de Jesús Perea-Flores, M.; Mendoza-Pérez, J. A. Identification of microplastics and associated contaminants using ultra high resolution microscopic and spectroscopic techniques. *Sci. Total Environ.* **2022**, *828*, 154434.
- (52) Tang, Z.; Zhu, F.; Jiang, T.; Wei, F.; Gao, Y.; Xiang, C.; Duan, Y.; Hua, Y.; Zhou, S.; Wang, Y. Oxygen-containing functional groups enhance uranium adsorption by aged polystyrene microplastics: Experimental and theoretical perspectives. *Chem. Eng. J.* **2023**, *465*, 142730.
- (53) Tang, S.; Lin, L.; Wang, X.; Yu, A.; Sun, X. Interfacial interactions between collected nylon microplastics and three divalent metal ions (Cu (II), Ni (II), Zn (II)) in aqueous solutions. *J. Hazard. Mater.* **2021**, *403*, 123548.
- (54) Omorogie, M. O.; Babalola, J. O.; Unuabonah, E. I.; Gong, J. R. Hybrid materials from agro-waste and nanoparticles: implications on the kinetics of the adsorption of inorganic pollutants. *Environ. Technol.* **2014**, *35*, 611–619.
- (55) Omorogie, M. O.; Babalola, J. O.; Unuabonah, E. I.; Song, W.; Gong, J. R. Efficient chromium abstraction from aqueous solution using a low-cost biosorbent: *Nauclea diderrichii* seed biomass waste. *J. Saudi Chem. Soc.* **2016**, *20*, 49–57.
- (56) Mohamed Nasser, S.; Abbas, M.; Trari, M. Understanding the rate-limiting step adsorption kinetics onto biomaterials for mechanism adsorption control. *Prog. React. Kinet. Mech.* **2024**, *49*, 14686783241226858.
- (57) Babalar, M.; Siddiqua, S.; Sakr, M. A. A novel polymer coated magnetic activated biochar-zeolite composite for adsorption of polystyrene microplastics: Synthesis, characterization, adsorption and regeneration performance. *Sep. Purif. Technol.* **2024**, *331*, 125582.
- (58) Karunattu Sajan, M.; Kirubalan, M. R.; Rajendran, A. S.; Natesan, A. L. F. Exploring the effective adsorption of polystyrene microplastics from aqueous solution with magnetically separable nickel/reduced graphene oxide (Ni/rGO) nanocomposite. *Environ. Sci. Pollut. Res.* **2024**, *31*, 38099–38116.
- (59) Al-Ghouti, M. A.; Da'ana, D. A. Guidelines for the use and interpretation of adsorption isotherm models: A review. *J. Hazard. Mater.* **2020**, *393*, 122383.
- (60) Kalam, S.; Abu-Khamsin, S. A.; Kamal, M. S.; Patil, S. Surfactant adsorption isotherms: A review. *ACS Omega* **2021**, *6*, 32342–32348.
- (61) Chen, X.; Hossain, M. F.; Duan, C.; Lu, J.; Tsang, Y. F.; Islam, M. S.; Zhou, Y. Isotherm models for adsorption of heavy metals from water—a review. *Chemosphere* **2022**, *307*, 135545.
- (62) Wang, J.; Sun, C.; Huang, Q.-X.; Chi, Y.; Yan, J.-H. Adsorption and thermal degradation of microplastics from aqueous solutions by Mg/Zn modified magnetic biochars. *J. Hazard. Mater.* **2021**, *419*, 126486.
- (63) Zhu, N.; Yan, Q.; He, Y.; Wang, X.; Wei, Z.; Liang, D.; Yue, H.; Yun, Y.; Li, G.; Sang, N. Insights into the removal of polystyrene nanoplastics using the contaminated corncob-derived mesoporous biochar from mining area. *J. Hazard. Mater.* **2022**, *433*, 128756.
- (64) Zhao, H.; Wu, J.; Su, F.; He, X. Removal of polystyrene nanoplastics from aqueous solutions by a novel magnetic zeolite adsorbent. *Hum. Ecol. Risk Assess.: Int. J.* **2023**, *29*, 327–346.
- (65) Han, F.; Wang, Y.; An, S.-Y.; Liu, L.; Ma, L.-Q.; Yang, L.; Liu, S.-Y. Poly (dimethyldiallylammonium chloride)-modified magnetic bentonite for removal of polystyrene nanoplastics. *J. Environ. Chem. Eng.* **2024**, *12*, 114013.
- (66) Singh, N.; Khandelwal, N.; Ganie, Z. A.; Tiwari, E.; Darbha, G. K. Eco-friendly magnetic biochar: An effective trap for nanoplastics of varying surface functionality and size in the aqueous environment. *Chem. Eng. J.* **2021**, *418*, 129405.
- (67) Shi, Y.; Du, J.; Zhao, T.; Feng, B.; Bian, H.; Shan, S.; Meng, J.; Christie, P.; Wong, M. H.; Zhang, J. Removal of nanoplastics from aqueous solution by aggregation using reusable magnetic biochar modified with cetyltrimethylammonium bromide. *Environ. Pollut.* **2023**, *318*, 120897.
- (68) Arenas, L. R.; Gentile, S. R.; Zimmermann, S.; Stoll, S. Nanoplastics adsorption and removal efficiency by granular activated carbon used in drinking water treatment process. *Sci. Total Environ.* **2021**, *791*, 148175.
- (69) Luo, D.; Wang, L.; Nan, H.; Cao, Y.; Wang, H.; Kumar, T. V.; Wang, C. Phosphorus adsorption by functionalized biochar: A review. *Environ. Chem. Lett.* **2023**, *21*, 497–524.
- (70) Omorogie, M. O.; Helmreich, B. Exploring the Potential of Amino-Functionalized Zeolite Series/H₃PO₄-Biochar for Environmental Microplastic Removal. *Ind. Eng. Chem. Res.* **2024**, *63*, 3947–3961.

(71) Sun, C.; Wang, Z.; Zheng, H.; Chen, L.; Li, F. Biodegradable and re-usable sponge materials made from chitin for efficient removal of microplastics. *J. Hazard. Mater.* **2021**, *420*, 126599.

(72) Zhao, H.; Huang, X.; Wang, L.; Zhao, X.; Yan, F.; Yang, Y.; Li, G.; Gao, P.; Ji, P. Removal of polystyrene nanoplastics from aqueous solutions using a novel magnetic material: Adsorbability, mechanism, and reusability. *Chem. Eng. J.* **2022**, *430*, 133122.

(73) Li, S.; Yang, M.; Wang, H.; Jiang, Y. Adsorption of microplastics on aquifer media: Effects of the action time, initial concentration, ionic strength, ionic types and dissolved organic matter. *Environ. Pollut.* **2022**, *308*, 119482.

(74) Huang, Z.; Bu, J.; Wang, H. Application of two modified kaolin materials in removing micro-plastics from water. *J. Mater. Cycles Waste Manage.* **2022**, *24*, 1460–1475.

(75) Ganie, Z. A.; Khandelwal, N.; Tiwari, E.; Singh, N.; Darbha, G. K. Biochar-facilitated remediation of nanoplastic contaminated water: Effect of pyrolysis temperature induced surface modifications. *J. Hazard. Mater.* **2021**, *417*, 126096.

(76) Shen, M.; Song, B.; Zeng, G.; Zhang, Y.; Teng, F.; Zhou, C. Surfactant changes lead adsorption behaviors and mechanisms on microplastics. *Chem. Eng. J.* **2021**, *405*, 126989.

(77) Anastopoulos, I.; Giannakoudakis, D. A.; Fronstistis, Z.; Zorpas, A. A.; Pashalidis, I.; Triantafyllidis, K. Biomass-derived adsorbents: Universal database development for their synthesis and remediation efficiency as a necessary step to move from laboratory-to pilot-scale applications. *Curr. Opin. Green Sustainable Chem.* **2024**, *47*, 100902.

(78) Momina; Ahmad, K. Feasibility of the adsorption as a process for its large scale adoption across industries for the treatment of wastewater: Research gaps and economic assessment. *J. Cleaner Prod.* **2023**, *388*, 136014.

(79) Baskar, A. V.; Bolan, N.; Hoang, S. A.; Sooriyakumar, P.; Kumar, M.; Singh, L.; Jasemizad, T.; Padhye, L. P.; Singh, G.; Vinu, A.; et al. Recovery, regeneration and sustainable management of spent adsorbents from wastewater treatment streams: A review. *Sci. Total Environ.* **2022**, *822*, 153555.